A note on the shoaling of acoustic–gravity waves

USAMA KADRI and MICHAEL STIASSNIE
Technion – Israel Institute of Technology
Faculty of Civil and Environmental Engineering
Technion 32000, Haifa
ISRAEL
usama.kadri@gmail.com
miky@technion.ac.il

Abstract: A mathematical solution of the two dimensional linear problem of an acoustic–gravity wave propagating over a rigid and slowly-varying bathymetry, in an acoustically homogeneous and slightly compressible ocean, is presented. Expressions for the far and near flow fields are derived. The present note enriches our knowledge about acoustic–gravity waves in a way that could assist, among others, in the early detection of tsunami.

Key–Words: Acoustic–gravity waves, shoaling, turning point, early detection of tsunami

1 Introduction

Most studies of ocean surface–waves neglect the small compressibility of the water. This approach is justified for many physical applications, but no for all. In an incompressible ocean, with constant depth, h, any given frequency ω corresponds to one progressive *gravity* wave with wave–number k. If the small compressibility of the water is taken into account, any given frequency ω corresponds to several progressive waves, with wave–numbers k_n, $n = 0, 1, ..., N$. The wave–number k_0 is almost identical to k, whereas $k_N < k_{N-1} < ... < k_2 < k_1 << k_0$. The additional waves $(k_1, ..., k_N)$ are called acoustic–gravity waves, and N is the nearest integer smaller than $(\omega h/\pi c_s + 1/2)$, where c_s is the speed of sound in water.

Acoustic–gravity waves are generated in the oceans all the time, as a result of nonlinear interactions of pairs of nearly opposing gravity–waves having equal or nearly equal frequencies, see [2], [1], [5], and references therein. Particularly energetic acoustic–gravity waves appear as a result of submarine earthquake, see [9], chapter 3.

The term *wave shoaling* refers to the two–dimensional problem (one horizontal dimension x) of waves propagating at normal incidence to straight parallel depth contours, usually in the shoreward direction. Assuming a slowly varying bathimetry, i.e. $\mu = (\mathrm{d}h/\mathrm{d}x)/(k_n h) << 1$; one can use a WKB approach, for which the constant depth solution is valid locally to obtain: (i) that $\omega = constant$, (thus k_n is given by the linear dispersion–relation); and (ii) that the energy–flux $F_n = constant$; see [11], chapter 3.

The energy flux is the product of the energy density E_n and the group–velocity $C_{g,n}$ (to be distinguished from the phase velocity $C_n = \omega/k_n$).

For gravity waves, both $C_{g,0}$ and C_0 are real for any depth, and tend to zero as the depth h tends to zero. As a result, the wave–steepness tends to infinity and gravity waves break in coastal–water (usually with minor reflection). For acoustic–gravity waves, the shoaling scenario is very different: (i) their group–velocity $C_{g,n}$ is real and decreases with the decrease of depth until it reaches zero at some finite depth $h_0^{(n)}$; (ii) their phase–velocity C_n is real and increases with the decrease of depth tending to infinity at the same depth $h_0^{(n)}$ (for depths smaller than h_0: C_n and the wave–number k_n are imaginary). In mathematical terms the point $x_0^{(n)}$, for which $h(x_0^{(n)}) = h_0^{(n)}$, is a *turning point*, which causes complete reflection, and requires special local treatment.

In this paper we present a mathematical solution of the two dimensional linear problem of an acoustic–gravity wave propagating over a rigid and slowly-varying bathimetry, in an acoustically homogeneous and slightly compressible ocean. Results by this paper comprise a reference for comparison with a similar ongoing research in which the elasticity of the ocean bottom is not neglected. The formulation of the problem is given in section 2. Matched asymptotic calculations of the far and near flow fields are presented in section 3. The solution for the far and near fields, and the results are presented in section 4 and 5, respectively. Finally, concluding remarks are given in section 6.

2 Formulation and basics

Consider the two dimensional problem of a progressive acoustic–gravity wave mode, in an ideal compressible fluid, propagating over a gradually decreasing depth towards a turning point, located at $x = 0$. The objective is to find the surface wave elevation $z = \eta(x,t)$, as well as the bottom pressure in the neighbourhood of the turning point. To this end, it is necessary to solve for the flow velocity potential $\phi(x, z, t)$. The governing equation is the two dimensional wave equation

$$\frac{\partial^2 \phi}{\partial t^2} = c_s^2 \left[\frac{\partial^2 \phi}{\partial x^2} + \frac{\partial^2 \phi}{\partial z^2} \right], \qquad \text{on} -h < z < 0, \quad (1)$$

where c_s is the speed of sound. The bottom and the linearized free–surface boundary conditions are, respectively,

$$\frac{\partial \phi}{\partial z} + \frac{\partial h}{\partial x}\frac{\partial \phi}{\partial x} = 0, \qquad \text{on } z = -h(x), \quad (2)$$

and

$$\frac{\partial^2 \phi}{\partial t^2} + g\frac{\partial \phi}{\partial z} = 0, \qquad \text{on } z = 0. \quad (3)$$

where g is the acceleration due to gravity. Note that the specific solutions fulfil the zero velocity boundary condition, which is compatible with the mild bottom–slope assumption.

The free surface elevation and the bottom pressure are then given by

$$\eta(x,t) = \frac{1}{g}\frac{\partial \phi}{\partial t}, \qquad \text{on } z = 0, \quad (4)$$

and

$$p_b(x,t) = \rho_s \frac{\partial \phi}{\partial t}, \qquad \text{on } z = -h(x), \quad (5)$$

where ρ_s is the density of water at the free surface.

Assuming a slowly–varying bathymetry the solutions of Eqs. (1), (2), and (3), to leading order in μ, are:

$$\phi_n = \psi_n(x)\frac{\cos\left[\kappa_n(\mu x)[h(\mu x) + z]\right]}{\cos\left[\kappa_n(\mu x)h(\mu x)\right]}e^{-i\omega t}, \quad (6)$$

where $n = 0, 1, 2, ..., N$ and

$$\omega^2 = -g\kappa_n(\mu x)\tan\left[\kappa_n(\mu x)h(\mu x)\right], \quad (7)$$

and ψ_n satisfy

$$\frac{\mathrm{d}^2\psi_n}{\mathrm{d}x^2} + k_n^2\psi_n = 0, \quad (8)$$

and

$$k_n^2 = \frac{\omega^2}{c_s^2} - \kappa_n^2. \quad (9)$$

The index n is dropped in the sequel for the sake of brevity. The solution of Eq. (8), which represents shoaling waves, is given by

$$\psi = A(\mu x)e^{i\int_0^x k(\mu x)\mathrm{d}x}. \quad (10)$$

To find the 'amplitude' A, one applies the following constant energy–flux condition:

$$F(x) = \frac{\rho_s}{4g}\frac{\omega^3 k}{\kappa^2}\left(1 + \frac{2\kappa h}{\sin(2\kappa h)}\right)|A|^2 = F(-L), \quad (11)$$

where $F(-L)$ is the input flux, at the point $x = -L$, for which $h(-L) \equiv h_L$ and $A(-L) \equiv A_L$, is given. The expression for the flux, given in Eq. (11), can be obtained from [15].

The above approach fails at the turning point where k becomes zero, leading to infinite values of the amplitude A. Physically, this means either wave–breaking, or wave reflection.

In the following section we use a matched asymptotic method to obtain a solution which is finite for all x, and produces complete reflection.

3 Matched asymptotic calculations

From Eqs. (7) and (9) one can show that the depth at the turning point of the nth mode is

$$h_0 \simeq \left(n - \frac{1}{2}\right)\pi\frac{c_s}{\omega}, \qquad n = 1, 2, 3, ... \quad (12)$$

Fig. 1 gives the values of h_0 in meters as function of frequency $f = \omega/2\pi$ in Hz for the three first modes, $n = 1, 2, 3$. In the sequel we focus on the first mode, without loss of generality.

3.1 Far field

A solution of Eq. (8) similar to Eq. (10), but with waves travelling in both directions, is given by

$$\psi = \frac{r(h)}{k^{1/2}}\left(A_L e^{i\int_0^x k\mathrm{d}x} + B_L e^{-i\int_0^x k\mathrm{d}x}\right), \quad (13)$$

where B_L is a second unknown constant, and Eq. (11) gives

$$\frac{r(h)}{k^{1/2}} = \frac{\kappa}{\kappa_L}\left(\frac{k_L}{k}\frac{\sin(2\kappa h)}{\sin(2\kappa_L h_L)}\frac{\sin(2\kappa_L h_L) + 2\kappa_L h_L}{\sin(2\kappa h) + 2\kappa h}\right)^{1/2}. \quad (14)$$

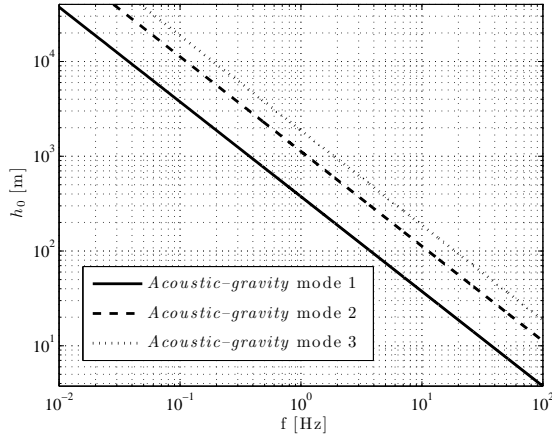Note that $r(h)/k^{1/2}$ tends to infinity at the turning point, and to unity at $x = -L$.

Figure 1: Turning point depth h_0 as function of the wave frequency $f = \omega/2\pi$, for the first three acoustic–gravity modes denoted by solid, dashed, and dotted lines, respectively.

3.2 Near field

A Taylor expansion of k^2 in the neighbourhood of the turning point gives

$$k^2 = k^2|_{h_0} + \frac{\mathrm{d}(k^2)}{\mathrm{d}h}|_{h_0}(h-h_0)+... \simeq -b_0 s_0 x, \quad (15)$$

where s_0 is the bottom slope at the turning point, and

$$b_0 = \frac{\mathrm{d}(k^2)}{\mathrm{d}h}|_{h_0} > 0. \quad (16)$$

From Eqs. (7) and (9) we write (for the first acoustic–gravity wave mode)

$$k^2 \simeq -\frac{\pi^2}{4h^2} + \frac{\omega^2}{c_s^2}. \quad (17)$$

Differentiation with respect to h and making use of Eq. (16) gives

$$b_0 = \frac{\pi^2}{2h_0^3}. \quad (18)$$

Substituting Eq. (15) into Eq. (8) leads to the Airy equation

$$\frac{\mathrm{d}^2\psi}{\mathrm{d}\sigma^2} - \sigma\psi = 0, \quad (19)$$

with

$$\sigma = (b_0 s_0)^{1/3} x. \quad (20)$$

Discarding the diverging solution of the Airy equation we obtain

$$\psi = c\mathrm{A_i}(\sigma), \quad (21)$$

where c is yet an unknown constant, and $\mathrm{A_i}$ is the Airy function.

3.3 Matching the far and the near fields

Using the asymptotic expression for the Airy function as $\sigma \to -\infty$, the near field solution, Eq. (21) gives

$$\psi = \frac{c}{2i\pi^{1/2}}(-\sigma)^{-1/4}$$
$$\times \left(e^{i\left(\frac{2}{3}(-\sigma)^{3/2}+\frac{\pi}{4}\right)} - e^{-i\left(\frac{2}{3}(-\sigma)^{3/2}+\frac{\pi}{4}\right)}\right). \quad (22)$$

Taking $x \to 0^-$ in the far field solution Eq. (13) and using Eq. (17) gives

$$\psi = \frac{r_0}{(b_0 s_0)^{1/6}}(-\sigma)^{-1/4}$$
$$\times \left(A_L e^{-i\frac{2}{3}(-\sigma)^{3/2}} + B_L e^{i\frac{2}{3}(-\sigma)^{3/2}}\right). \quad (23)$$

where $r_0 = r(h_0)$.

Matching Eqs. (22) and (23) gives the values of the two unknowns

$$c = -2i\pi^{1/2}\frac{A_L r_0}{b_0 s_0^{1/6}}e^{i\frac{\pi}{4}}, \quad (24)$$

and

$$B_L = -A_L e^{i\frac{\pi}{2}}. \quad (25)$$

4 Solution

4.1 Solution for the far field

Substituting Eq. (25) into Eq. (13), and Eq. (13) into Eq. (6) and taking the real part gives the far field solution of the velocity potential

$$\phi(x,z,t) = -\frac{gH}{\omega}\frac{r(h)}{k^{1/2}}\frac{\cos[\kappa(z+h)]}{\cos(\kappa h)}$$
$$\times \cos\left(\int_0^x k dx + \frac{\pi}{4}\right)\cos\left(\omega t + \frac{\pi}{4}\right), \quad (26)$$

where $H = -2\omega g A_L$ is the **height** of the incident wave at $x = -L$.

The surface wave elevation given by Eq. (4) becomes

$$\eta(x,t) = H\frac{r(h)}{k^{1/2}}\cos\left(\int_0^x k dx + \frac{\pi}{4}\right)$$
$$\times \sin\left(\omega t + \frac{\pi}{4}\right). \quad (27)$$

Using Eqs. (5) and (26), and substituting $z = -h$, the dynamic bottom pressure p_b is given by

$$p_b(x,t) = \frac{\rho_s gH}{\cos(\kappa h)}\frac{r(h)}{k^{1/2}}\cos\left(\int_0^x k dx + \frac{\pi}{4}\right)$$
$$\times \sin\left(\omega t + \frac{\pi}{4}\right). \quad (28)$$

4.2 Solution for the near field

Substituting Eq. (24) into Eq. (21), and taking the real part gives the near field solution of the velocity potential

$$\phi(x,z,t) = -\frac{gH}{\omega}\frac{r_0\pi^{1/2}}{(b_0 s_0)^{1/6}}\frac{\cos[\kappa(z+h)]}{\cos(\kappa h)}$$
$$\times \mathrm{Ai}\left((b_0 s_0)^{1/3}x\right)\cos\left(\omega t + \frac{\pi}{4}\right), \qquad (29)$$

with the surface elevation

$$\eta(x,t) = H\frac{r_0\pi^{1/2}}{(b_0 s_0)^{1/6}}\mathrm{Ai}\left((b_0 s_0)^{1/3}x\right)$$
$$\times \sin\left(\omega t + \frac{\pi}{4}\right), \qquad (30)$$

and the dynamic bottom pressure

$$p_b(x,t) = \frac{\rho_s gH}{\cos(\kappa h)}\frac{r_0\pi^{1/2}}{(b_0 s_0)^{1/6}}\mathrm{Ai}\left((b_0 s_0)^{1/3}x\right)$$
$$\times \sin\left(\omega t + \frac{\pi}{4}\right). \qquad (31)$$

4.3 Pressure amplification factor

A convenient way to monitor acoustic–gravity waves is by measuring the water pressure near the bottom of the sea. The variation of the bottom pressure with depth, normalized by the bottom pressure at $x = -L$ is given, from Eqs. (28) and (31), by

$$A_F = \begin{cases} \left[\dfrac{p_b(h)}{p_b(h_L)}\right]_{\text{Far field}}, & -h_L \leq h \leq h_m \\[2em] \dfrac{[p_b(h)]_{\text{Near field}}}{[p_b(h_L)]_{\text{Far field}}}, & -h_m \leq h \end{cases}$$
$$(32)$$

where h_m is the depth at which the far field and the near field solutions match.

5 Results

5.1 Matching the far and the near fields

The general solution for shoaling is governed by matching the far and the near field solutions (i.e., matching Eqs. (26), (27) and (28), with Eqs. (29), (30) and (31), respectively). Fig. 2 presents the general solution of the normalized surface elevation η/H (top), and the bottom pressure $p_b/(\rho_s gH)$ (middle) as function of water depth h. A zoom in on the matching zone for the normalized surface elevation is presented in the bottom plot. Fig. 2 captures both the matching
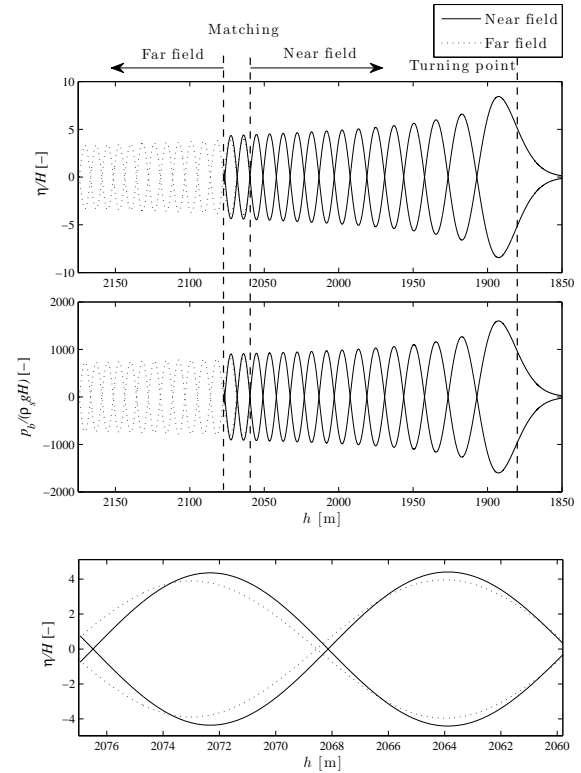

Figure 2: Matching the far field (dotted–lines) with the near field (solid lines) as function of depth h. Top: normalized surface elevation η/H. Middle: normalized dynamic bottom pressure $p_b/(\rho_s gH)$. Bottom: zoom–in on the matching of the normalized surface elevation. Prescribed frequency $f = 0.2$ Hz. Seabed slope at the vicinity of the turning point $s_0 = 0.001$. Ocean depth is $h_L = 4000$ m.

and the near field solution near the turning point. In the figure, the dotted and solid curves represent the far and near field solutions, respectively. The numerical results shown in Fig. 2 were obtained by considering the first acoustic–gravity mode with a prescribed frequency $f = 0.2$ Hz ($\omega = 2\pi f = 1.256$ rad/s), ocean depth of $h = 4000$ m, and a local slope of $s_0 = 0.001$ near the turning point. The results show satisfactory matching solutions. The matching occurs several wave lengths prior to the turning point. As expected, the amplitudes increased as the depth decreased, reaching a maximum value in the neighbourhood of the turning point. At the turning point the mode is reflected, and the amplitudes rapidly decay as the depth is further decreased.

The wave height H of the acoustic–gravity wave can be estimated by the interaction of two gravity waves nearly opposing and propagating each at fre-

Table 1: Properties of typical gravity and acoustic–gravity waves; $h = 4000$ m, g=10 m/s^2, $c_s = 1500$ m/s; T_g, f_g and λ_g are the period, frequency and wavelength of the gravity wave; f, and λ are the frequency and wavelength of the acoustic–gravity wave.

T_g[s]	f_g[1/s]	λ_g [m]	f[1/s]	λ[m]
1.33	0.75	2.83	1.5	1,000
3	0.33	14.6	0.66	2,300
10	0.1	159	0.2	8,500
20	0.05	636	0.1	45,000

quency $\approx \omega/2$, as originally proposed by [10] and later by [6] and [8]. From[10] (section 4) we assess that

$$H = a_1 a_2 \frac{\omega^2}{4g}, \qquad (33)$$

where a_1 and a_2 are the amplitudes of the two interacting gravity waves. Choosing $a_1 = a_2 = 0.5$ m, which is a typical wave amplitude in the deep ocean, yields $H = 0.01$ m. Thus, from Fig. 2 we find that an acoustic–gravity wave with an initial wave–height of 0.01 m reaches a maximum of 0.084 (amplification factor of 8.4) near the turning point. Similarly, the bottom pressure which at $h_L = 4000$ m is $p_b = 40$ kPa (≈ 0.39 atm) reaches a maximum of $p_b = 160$ kPa (≈ 1.58 atm) near the turning point – an amplification factor A_F of about four. A gravity wave with period $T_g = 10$ s (frequency $f_g = f/2 = 0.1$ s^{-1}) has a wavelength of $\lambda_g = 159$ m, which is significantly smaller than the length of the generated acoustic–gravity wave $\lambda = 8.5$ km (at $h_L = 4000$ m). A comparison between properties of gravity and acoustic–gravity waves at $h_L = 4000$ m, is summarized in Table 1.

Note that the choice of h_L and f was not arbitrary. The choice of $h_L = 4000$ m represents a typical average depth of the deep ocean, and $f = 0.2$ Hz was chosen within the region of the highest spectral levels which are generated by wave–wave interactions (see [5]).

5.2 Effect of the bottom slope near the turning point

The maximum amplitude height (e.g. for surface elevation), as well as the depth at which the maximum height is obtained is affected both by the bottom slope and by the prescribed mode frequency, as shown in
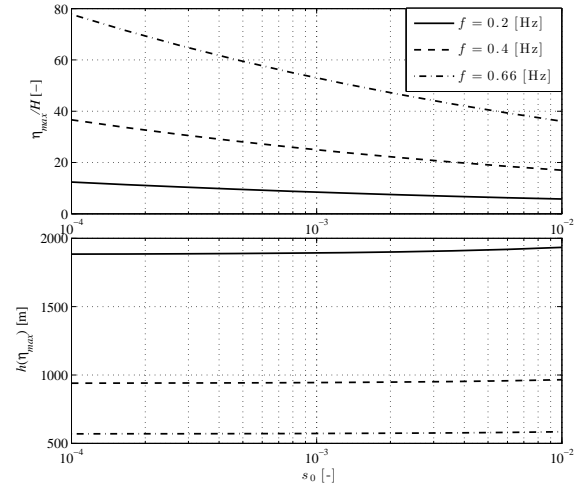

Figure 3: Effect of the seabed slope s_0 on the maximum surface elevation η_{max} (top) and the depth at maximum $h(\eta_{max})$ (bottom). Solid, dashed, and dashed–dotted lines denote a frequency of $f = 0.2$, 0.4, and 0.66 Hz, respectively. Ocean depth is $h_L = 4000$ m.

Fig. 3. The upper and bottom subplots of Fig. 3 present the maximum surface elevation, and its location (in h), respectively. The solid, dashed, and dashed–dotted lines are for $f = 0.2$, 0.4, and 0.66 Hz, respectively. It is found that while the maximum surface elevation η_{max} monotonically decreases with the slope s_0, its location $h(\eta_{max})$ only slightly increase. However, increasing the frequency results in a larger maximum elevation, occurring at a shallower water.

5.3 Pressure amplification factor

Fig. 4 (top) shows the *envelope* of the far field solution of the bottom pressure amplification factor A_F as function of the mode frequency spectrum, at a given depth $h_0 = 250$ m. The calculations were carried out with $s_0 = 0.001$. The far field solution is not valid in the neighbourhood of $f(h_0)$, where $h_0 = 250$ m is the turning point. At larger frequencies, it is found that A_F increases with the frequency (provided that H is similar for all frequencies). The shaded area is magnified in Fig. 4 (bottom) to allow comparison with the near field solution.

The near field solution provides a detailed behaviour of A_F in the neighbourhood of $f(h_0)$ as presented in Fig. 4 (bottom). A maximum is achieved around $f = 1.51$ Hz, and rapidly decreases as the frequency $f < 1.51$ Hz decrease. Note that the periodic
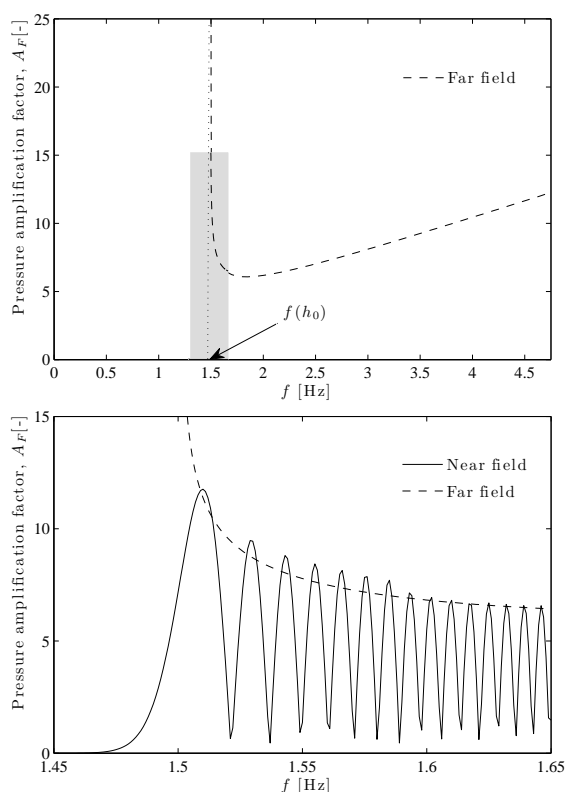
Figure 4: Top: envelope of the far field solution (dashed–line) for the dynamic bottom pressure amplification factor A_F as function of frequency $f = \omega/2\pi$, at a constant depth $h_0 = 250$ m. Local seabed slope $s_0 = 0.001$. Ocean depth is $h_L = 4000$ m. Bottom: zoom–in on the shaded area, with the envelope of the far field solution (dashed–line), and the near field solution (solid line).

behaviour of A_F is due to the fact that the reflected waves, each at its turning point, are actually standing waves.

6 Concluding Remarks

The two dimensional shoaling problem of an acoustic–gravity wave mode propagating over a slowly varying bathymetry with a linear slope in an inviscid and slightly compressible fluid has been addressed. The existence of acoustic–gravity modes depends on water depth, h, and the frequency of propagation ω. Each wave is reflected at the corresponding turning point, forming a standing wave.

6.1 Far from the turning point

Far from the turning point the solution for a given depth and modal frequency is governed by conservation of energy flux between the deep ocean (h_L) and the given depth (h), where the actual bottom topography and distance do no affect the solution (assuming no energy losses, e.g. due to bottom friction). In the far field solution the wave amplitude increases as water becomes shallower. At a given depth, the amplitude amplification factor increases with the frequency.

6.2 At the vicinity of the turning point

The far field solution is singular at the turning point, and thus fails to describe the evolution of waves at the vicinity of the turning point. Alternatively, the near field solution is governed by the Airy function. For each prescribed frequency, the near field solution results in amplified amplitudes reaching a maximum in the neighbourhood of the turning point, and a rapid decay thereafter. Thus, at a given depth one could expect a frequency spectrum dominated by the most amplified amplitudes.

6.3 Early detection of tsunami

The choice of $h_L = 4000$ m is appropriate both for the *2004 Boxing Day* tsunami and the *1960 Chile* tsunami (e.g. [4]). In both occurrences the gravity wave propagated with a velocity of about 200 m/s, which is considerably smaller than the velocity of the acoustic–gravity waves. Therefore, the capability to measure the acoustic–gravity modes should be considered for early detection of tsunami as proposed, among others, by [3] and [12]. [7] claimed that the dynamic bottom pressure could be sufficiently large for measurement purposes. However, they wondered on the optimal location of measurement sensors. In this context, the current work provides a first step for calculating frequency spectra as function of depth, by indicating the range of frequencies to be expected at the chosen depth; namely the frequencies for which the amplified amplitudes are the largest.

6.4 Non–rigid bottom

This paper provides a (rigid–bottom) limit solution of the general problem where the elasticity of the ocean bottom is not neglected. Considering the elasticity of the bottom, which is currently an ongoing research, results in *Rayleigh* or *Scholte* type of waves (e.g.,

see [14]; [13]), and thus important for discussing the properties of real waves measured in the ocean.

Acknowledgment

References:

[1] Ardhuin, F., A. Balanche, E. Stutzmann, and M. Obrebski, 2012: From seismic noise to ocean wave parameters: General methods and validation. *J. Geophys. Res.*, **117**, C05002, doi:10.1029/2011JC007449.

[2] Ardhuin, F., E. Stutzmann, M. Schimmel, and A. Mangeney, 2011: Ocean wave sources of seismic noise, *J. Geophys. Res..* **116**, C09004, doi:10.1029/2011JC006952.

[3] Chierici, F., L. Pignagnoli, E. and Davide, 2010: Modeling of the hydroacoustic signal and tsunami wave generated by seafloor motion including a porous seabed. *J. Geophys. Res.*, **115**, C03015, doi:10.1029/2009JC005522.

[4] Constantin, A., and R.S. Johnson, 2008: Propagation of very long water waves, with vorticity, over variable depth, with applications to tsunamis. *Fluid Dyn. Res.*, **40**, 175–211.

[5] Duennebier, F. K., R. Lukas, E.-M. Nosal, J. Aucan, and R. A. Weller, 2012: Wind, waves, and acoustic background levels at Station ALOHA. *J. Geophys. Res.*, **117**, C03017, doi:10.1029/2011JC007267.

[6] Hasselmann, K., 1963: A statistical analysis of the generation of microseisms. *Rev. Geophys.*, **1**, 177-210, doi:10.1029/RG001i002p00177.

[7] Kadri, U., and M. Stiassnie, 2012: Acoustic–Gravity waves interacting with the shelf break, *J. Geophys. Res.*, **117**, C03035, doi:10.1029/2011JC007674

[8] Kibblewhite, A. C., and C. Y. Wu (Eds.), 1996: *Wave Interactions as a Seismo–acoustic Source*. Springer, Berlin, 313 pp., doi:10.1007/BFb0011210.

[9] Levin, B., and M. Nosov, 2009: *Physics of Tsunamis. Springer Verlag, Heidelberg*, 327 pp.

[10] Longuet–Higgins, M. S., 1950: A theory of the origin of microseisms. *Philos. Trans. R. Soc. London, Ser. A*, **243**, 1-35, doi:10.1098/rsta.1950.0012.

[11] Mei, C. C., M. Stiassnie, and D.K.-P. Yue, 2005: *Theory and Applications of Ocean Surface Waves. Part 1: Linear Aspects*. World Scientific Publishing Co. Pte. Ltd., 506 pp.

[12] Stiassnie, M., 2010: Tsunamis and acoustic–gravity waves from underwater earthquakes. *J. Eng. Math.*, **67**, 23–32.

[13] Stoneley, R., 1926: The effect of the ocean on Rayleigh waves. *Mon. Not. Roy. Astron. Soc. Geophys. Suppl.*, **1**, 349–356.

[14] Webb, S. C., and A. Schultz, 1992: Very low frequency ambient noise at the seafloor under the Beaufort sea icecap. *J. Acoust. Soc. Amer.*, 91 **3**, 1429-1439.

[15] Yamamoto, T., 1982: Gravity waves and acoustic waves generated by submarine earthquakes. *Soil dyn. Earthq. Eng.*, **1**, 75-82.